Enhanced vibrational solvatochromism and spectral diffusion by electron rich substituents on small molecule silanes

Courtney M. Olson, Adam Grofe, Christopher J. Huber, Ivan C. Spector, Jiali Gao, and Aaron M. Massari

Citation: The Journal of Chemical Physics **147**, 124302 (2017);
View online: https://doi.org/10.1063/1.5003908
View Table of Contents: http://aip.scitation.org/toc/jcp/147/12
Published by the American Institute of Physics

Enhanced vibrational solvatochromism and spectral diffusion by electron rich substituents on small molecule silanes

Courtney M. Olson,[1] Adam Grofe,[1] Christopher J. Huber,[2] Ivan C. Spector,[1] Jiali Gao,[1,3] and Aaron M. Massari[1,a)]

[1]*Department of Chemistry, University of Minnesota–Twin Cities, Minneapolis, Minnesota 55455, USA*
[2]*Doane University, 1014 Boswell Avenue, Crete, Nebraska 68333, USA*
[3]*Theoretical Chemistry Institute, Jilin University, Changchun, Jilin Province 130023, People's Republic of China*

(Received 19 May 2017; accepted 8 September 2017; published online 25 September 2017)

Fourier transform infrared and two-dimensional IR (2D-IR) spectroscopies were applied to two different silanes in three different solvents. The selected solutes exhibit different degrees of vibrational solvatochromism for the Si–H vibration. Density functional theory calculations confirm that this difference in sensitivity is the result of higher mode polarization with more electron withdrawing ligands. This mode sensitivity also affects the extent of spectral diffusion experienced by the silane vibration, offering a potential route to simultaneously optimize the sensitivity of vibrational probes in both steady-state and time-resolved measurements. Frequency-frequency correlation functions obtained by 2D-IR show that both solutes experience dynamics on similar time scales and are consistent with a picture in which weakly interacting solvents produce faster, more homogeneous fluctuations. Molecular dynamics simulations confirm that the frequency-frequency correlation function obtained by 2D-IR is sensitive to the presence of hydrogen bonding dynamics in the surrounding solvation shell. *Published by AIP Publishing.* https://doi.org/10.1063/1.5003908

I. INTRODUCTION

Solvent motions play a critical role in chemical reactivity and solvation dynamics.[1–4] Perhaps the most obvious example is found in electron transfer reactions in which solvent shell dynamics contribute the energy needed to reach the transition state geometries of the donor and acceptor species.[5,6] In fact, for any condensed phase reaction, solvent-solute interactions can stabilize or destabilize the transition state, thereby directly influencing the rate coefficient.[7–11] For example, in biomacromolecules, key structural motions for the function of proteins or enzymes can be slaved to the dynamics of the surrounding solvation layer.[12–17] Likewise, catalytic rate constants are always specific to a solvent system,[18–21] and ultrafast dynamics in the solvation shell have been directly correlated with proposed mechanistic steps for organometallic catalysts.[22,23]

A variety of approaches have been used to characterize solvent dynamics.[24–35] All of these techniques report some facet of solvent motions, but none of them delivers the full dynamic picture. Complete structural evolution is filtered by the sensitivity of the reporter to each dynamic component, and only a subset of the coupled dynamics is visible through the lens of a particular measurement technique. For example, two-dimensional infrared (2D-IR) spectroscopy monitors the time dependent frequency fluctuations of a vibrational mode on a solvated solute species.[31–34,36] Changes in the vibrational frequency are dependent on the time scales of solvent motions in the proximal solvation shell and the degree to which those motions perturb the vibrations of the solute. The latter effect depends on solvent polarity and the strength of solute-solvent interactions—generally only the closest solvation shells exert a measurable influence on frequency fluctuations of the solute.[1,2,4,23] Therefore, the 2D-IR spectrum of a particular solute vibrational mode is blind to solvent motions in the bulk and even excludes dynamics in the solvation shell that do not perturb its vibrational frequency. In this context, molecular dynamics (MD) simulations can complement experimental measurements to provide detailed, structural insights into the microscopic mechanism of solvation.[14,37–46]

In this work, we report a combined experimental and computational investigation of vibrational solvatochromism and spectral diffusion in small silane molecules in various solvents using Fourier transform infrared (FTIR) and 2D-IR spectroscopies. To elucidate substituent effects on solvation dynamics, trimethoxysilane (TriMOS) and triphenylsilane (TriPS) were chosen in our study since the same vibrational mode can be monitored in the presence of different electron withdrawing ligands, giving rise to different solvatochromic responses. The study of these model molecules reveals the role of substituents on spectral diffusion in different solvents. The time scales and amplitudes of spectral diffusion are extracted from the 2D-IR data, which are further analyzed through molecular dynamics (MD) simulations in which each solute molecule is represented explicitly by a quantum mechanical method, embedded in the solvent environment approximated by a molecular mechanics force field. Such a combined QM/MM treatment of solute-solvent interactions allows a direct probe of the effect of solvent dynamics on the instantaneous change of the solute potential energy surface and its vibrational frequency as measured experimentally.

a)Author to whom correspondence should be addressed: massari@umn.edu.

II. EXPERIMENTAL METHODS

Trimethoxysilane (TriMOS, 95%, Sigma-Aldrich), triphenylsilane (TriPS, 97%, Sigma-Aldrich), chloroform (99.9% purity, anhydrous, Acros Organics), isopropanol (99.5%, anhydrous, Sigma-Aldrich), and pentane (*n*-pentane, 98%, Sigma-Aldrich) were used as received.

TriPS and TriMOS solutions were prepared in each solvent as 5 m/m % and 5 v/v % solutions, respectively, giving absorbances of 100–200 mOD for the Si–H vibration on both solutes. Solutions were used within 1 week of preparation. Spectroscopic studies were performed on solutions sandwiched between two 3 mm CaF_2 windows with a 50 μm Teflon spacer to define the sample path length.

Fourier transform infrared (FTIR) spectra were collected on a Nicolet 6700 FTIR spectrometer (Thermo Scientific) with at least 16 scans and a resolution of 1 cm^{-1}. A background spectrum of each of the solvents was subtracted from the respective TriMOS and TriPS spectra.

The 2D-IR instrument has been described previously.[47] The mid-IR pulses were tuned to the Si–H stretching frequency (2200 cm^{-1} for TriMOS and 2130 cm^{-1} for TriPS). All of the 2D-IR spectra were analyzed using the centerline slope (CLS) method and then iteratively fit with the linear line shape to obtain the frequency-frequency correlation function (FFCF) as a homogeneous term plus a sum of exponentials: $FFCF(t) = \frac{\delta(t)}{T_2} + \Delta_1^2 \exp(-t/\tau_1) + \Delta_2^2 \exp(-t/\tau_2)$.[48,49] IR pump-probe spectroscopy was carried out with the pump and probe beams polarized at the magic angle to remove contributions from orientational relaxation,[50] as described previously.[51] The data were fit from 1 to 75 ps to determine the population relaxation times (lifetime, T_1) for the v = 0-1 and 1-2 transitions. The vibrational relaxation times for these two transitions were consistently the same within errors, and the 0-1 values were used in data analyses. Additional details of 2D-IR and IR pump-probe measurements and the FFCF calculation process are provided in the supplementary material.

The computational analysis followed a two-pronged approach: (1) density functional theory (DFT) calculations were performed with two continuum solvation models using the M06-2X functional along with the 6-31+G(d,p) basis set and (2) combined quantum mechanical and molecular mechanical (QM/MM) simulations were carried out to understand the microscopic solvation dynamics of the vibrational chromophore. DFT calculations and subsequent analyses were performed using Gaussian 09.[52] The QM/MM simulations were performed using CHARMM,[53] in which the solute is treated by the semiempirical Austin model 1 (AM1) method[54] to provide an adequate sampling of the configuration space. For each solvent, the molecular dynamics were executed for 2 ns with a 1 fs integration time step under periodic boundary conditions at 1 atm and 25 °C. Coordinates were saved every 10 fs, resulting in a total of 200 000 configurations, which were used for all subsequent analyses. Further information on the computational details of MD simulations can be found in the supplementary material.

The instantaneous vibrational frequency of the silicon hydride mode at a given solvent configuration was determined using a vibration quantum-mechanical perturbation theory [quantum vibrational perturbation (QVP)] that was developed recently.[55] In this approach, the effects of solute-solvent interactions on the vibrational wave function and transition energies of the solute are treated as a perturbation to a reference state. In the present study, the reference vibrational state was the vibrational wave function at time zero after the initial equilibration for data collection (which can be regarded as an arbitrary moment in time during the MD simulation). Numerically, the wave function of the reference state was modeled using the potential optimized discrete variable representation (PO-DVR).[56–58] In this manner, the changes in the wave function for the ground state and the first two excited states due to the instantaneous solvent fluctuations as well as the change in solute geometry at future times were determined by perturbation theory. Although second-order perturbation yields sufficient precision (~1 cm^{-1}), we used the fourth-order perturbation theory (QVP4) thanks to the computational efficiency using the PO-DVR, which ensures that the computed vibrational frequencies are within 0.5 cm^{-1} of the exact result for each configuration. Because a discrete variable representation is employed, the calculation of the perturbation operator only requires single point energy calculations at the PO-DVR points without the need to explicitly solve the vibrational Schrödinger equation. Consequently, the QVP4 approach is computationally efficient, providing the instantaneous, on-the-fly transition energies of the solute for the 0-1 and 1-2 excitations. Importantly, nuclear quantum mechanical effects as well as solvent dynamics on the solute potential energy surface are explicitly included in the computation although nuclear quantum effects on solute-solvent coupling are neglected. A complimentary alternative approach is the widely used electrostatic potential mapping procedure. Further details concerning the determination and application of the normal mode are found in the supplementary material. Overall, the QVP4 calculations captured the time-dependent evolution of the vibration excitation energies of the solute, which were used to model the linear and nonlinear absorption spectra and the FFCF.[59]

The hydrogen bonding lifetime (τ_{HB}) of the solvent was determined by calculating the hydrogen bond correlation function,[60,61]

$$C(t) = \left\langle \frac{\sum h_{ij}(t_0) h_{ij}(t + t_0)}{\sum h_{ij}(t_o)^2} \right\rangle,$$

where $h_{ij}(t)$ is unity when the pair of solvent molecules *i* and *j* are hydrogen bonded, and zero otherwise. The computed correlation function was fitted to a set of three exponentials,[60–62] and the average τ_{HB} was determined by integrating the correlation function. For these calculations, a hydrogen bond was defined by geometrical criteria such that the donor-acceptor distance was less than 3.0 Å and the OH–O angle was greater than 130°. This methodology has been implemented into the MdAnalysis library in Python[62] and possibly underestimates the lifetime since it does not take into account instances of transient breaking and reforming of the same bond.

Before concluding this section, we make a distinction in the trajectories used to determine correlation functions. First, there is the molecular dynamics trajectory, which encompasses the entirety of the dataset from which the correlation

function is calculated. Second, there are correlation trajectories, which are a subset of the molecular dynamics trajectory, upon which the correlation function is averaged at each point in the correlation function. In the calculation of the hydrogen bond correlation function, correlation trajectories were only accepted if the hydrogen bond was continuous throughout the correlation trajectory. This could in principle underestimate the hydrogen bond lifetime because it does not include transient breaks of the hydrogen bond. However, this is compensated for by using generous hydrogen bond geometric criteria of 3 Å for the hydrogen-acceptor distance and 130° for the donor-hydrogen-acceptor angle. This algorithm was further modified to calculate the hydrogen bond lifetime at the solute-solvent interface by only including correlation trajectories that were within the first shell of the solvent. The first shell was determined by having any distance between the atoms of the solute and the atoms of each solvent molecule which is less than 6 Å, the minimum following the first peak of the radial distribution function (Fig. S14 of the supplementary material) between the central carbon of isopropanol and the hydride hydrogen.

III. RESULTS AND DISCUSSION

Figure 1 shows the solvent-subtracted FTIR spectra for the silicon hydride, Si–H, stretching vibration of TriMOS and TriPS in three different solvents: isopropanol, chloroform, and pentane. A most striking finding is the large substituent effect on the silane stretch mode; its vibrational frequency is blue-shifted by 74 cm^{-1} when the phenyl groups of TriPS are replaced with the electron-withdrawing substituents in TriMOS in the non-polar solvent pentane. The experimental influence of CH_3O-substitution on the Si–H frequency in pentane is reproduced by the computational results of 78 and 81 cm^{-1} using, respectively, the Minnesota solvation model (SMD)[63] and the polarizable continuum model (PCM)[64] at the M06-2X/6-31+G(d,p) level of theory (Table SII of the supplementary material). The corresponding change of 59 cm^{-1} was obtained from QM/MM molecular dynamics simulations (Table SIII of the supplementary material). The TriMOS hydride stretch frequency (ν_{Si-H}) also exhibits a strong hypsochromic change with absorption peak maxima

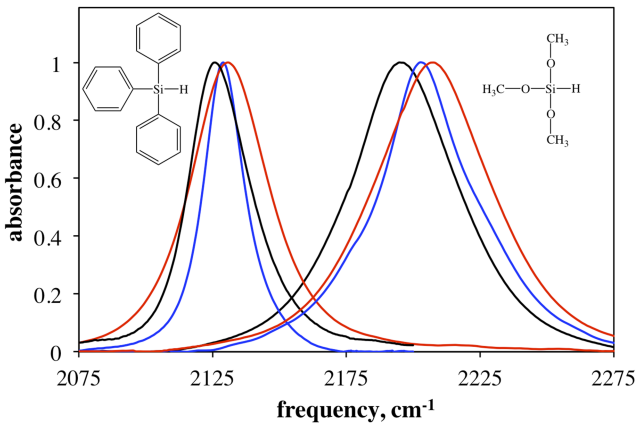

FIG. 1. Solvent subtracted, baselined, and normalized FTIR spectra of the Si–H vibration for TriPS (left) and TriMOS (right) in isopropanol (black), chloroform (red), and pentane (blue).

at 2194.6, 2203.2, and 2207.2 cm^{-1} in isopropanol, pentane, and chloroform, respectively. Similarly, the corresponding values for TriPS are 2125.7, 2129.2, and 2131.1 cm^{-1}. The experimental trend of the solvatochromic shift in the order of isopropanol < pentane < chloroform for ν_{Si-H} is surprising since it does not follow any solvent polarity scales. Continuum model calculations, explicit MD simulations, and experiments predict the vibrational frequency to decrease monotonically with the solvent polarity (polarity trend: pentane < chloroform < isopropanol), in accordance with the Stark effect.[65] Interestingly, although the trend is the same, TriMOS and TriPS experience different degrees of solvatochromism. It has been established that ν_{Si-H} is tuned by the inductive effect of the substituents.[66–70] A major difference between TriMOS and TriPS is the presence of electronegative oxygen atoms in the methoxy ligands that strongly polarize the Si–O bonds; the partial atomic charge on silicon changes from 0.08 *e* in TriPS to 1.03 *e* in TriMOS (Table SI of the supplementary material). Previous analysis showed that the hydrogen bonding ability of the solvent was correlated with solvatochromic shifts of ν_{Si-H} on silanes and silica sol-gels.[71] Consequently, we hypothesized that the solvent interactions with the oxygen atoms would have the greatest influence on the vibrational mode due to the inductive effect.[71,72] Yet, the fact that the solvatochromic trend in Fig. 1 is the same for TriPS, which lacks oxygen atoms in its ligands, indicates that the solvent influence is not limited to this specific interaction.

To gain insights into solvatochromism for TriMOS and TriPS, we modeled the ν_{Si-H} vibrations through a combination of DFT calculations on solutes using two continuum solvent models (SMD[63] and PCM[64]) and MD simulations. Continuum solvation methods introduce the equilibrium electric polarization into the Born-Oppenheimer surface, probing the Stark effect on the vibrational frequency, but the unusual trend of the Si–H vibrational frequency shifts observed experimentally was not fully reproduced by either continuum models (additional details in the supplementary material). In particular, the simulations yielded the correct relative frequency shifts for TriPS between pentane and chloroform solvents, but not in isopropanol, and for TriMOS, the order between pentane and isopropanol was correct, yet not in $CHCl_3$. We suspect that the large dispersion contributions from chloroform are partly responsible for the unusual experimental findings. The DFT/SMD calculations yielded a large blue shift for TriMOS in isopropanol, a clear departure from other computational methods and experiments. Nevertheless, the trends obtained using the PCM model and QM/MM simulations are in agreement with each other, suggesting that dielectric and electrostatic interactions are consistently represented. The SMD model includes contributions due to surface tension terms, which may be too sensitive in the Hessian for the present systems.

A plausible explanation for the unusual frequency trends is that specific solvent-solute interactions that were not captured by implicit solvent modeling might be needed to reproduce the experimental order of spectral change. In calculations with TriMOS, the inclusion of an explicit H-bond donor (methanol, see Table SIV of the supplementary material) near the oxygen atoms of the methoxy ligands was able to yield the red

spectral shift observed in isopropanol relative to that in pentane. Similarly, introducing an explicit $CHCl_3$ solvent molecule in the solvation shell of TriMOS led to a mild blue shift, which could be further enhanced by constraining the solvent geometry to maintain a halogen bonding configuration to the hydride (see Table SV of the supplementary material).[73,74] The fact that this configuration was not maintained for this single $CHCl_3$ molecule indicates that the halogen bond is not the most stable interaction; however, solvent packing effects in the condensed phase would lead to this interaction being more significant. In addition, the radial distribution functions between the hydrogen atom of the silane mode and the chlorine atom of chloroform (Fig. S13 of the supplementary material) in our simulations of both TriPS and TriMOS show a moderate peak at roughly the same distance as the halogen bond determined by the constrained QM geometry optimization. The integrals of the distribution peaks show that their occupations are greater than one, which suggests that on average the halogen bond is maintained through most of the simulations. We conclude that the unusual experimental solvatochromic trend for ν_{Si-H} is understood as arising from specific hydrogen and halogen bonding interactions with the solute. Given that solvatochromism is not fully reproduced from QM/MM suggests that non-electrostatic effects, such as dispersion and charge transfer, also play a role for $CHCl_3$.

An interesting finding from our analyses (supplementary material) is that the magnitudes of the partial atomic charges for silicon and hydrogen—the main components of the normal mode vector—increase with the electronegativity of the ligands (Table SII). This provides an explanation for the greater solvatochromic effects in TriMOS than in TriPS: the electron withdrawing methoxy ligands lead to a greater charge separation and electrostatic coupling to the solvent reaction field.[65] Consequently, the average dipole moment for TriMOS is increased from 1.8 D in pentane to 2.5 D in isopropanol, whereas the corresponding values are 0.8 and 1.2 D, respectively, for TriPS.

One key question is whether a change in solvatochromism correlates with increased sensitivity to ultrafast structural dynamics leading to spectral diffusion. If so, this would provide a strategy to designing vibrational probes with enhanced sensitivity to solvent dynamics by tuning peripheral ligands. As a starting point, we note that the FTIR peak widths vary considerably among the three solvents for both compounds, increasing in the order of pentane (blue) < isopropanol (black) < chloroform (red). The TriPS peak widths are generally narrower than those of TriMOS, though the broadening trend with solvent remains the same. The FTIR peak widths are influenced by the range of chemical environments as well as the time dependent fluctuations of the vibrational frequencies that are driven by solvent dynamics (spectral diffusion and homogeneous broadening). Broader peaks in more polar solvents suggest that their solvation environments are more heterogeneous and/or dynamic than that of pentane. 2D-IR spectroscopy enables one to decompose the FTIR line shapes into their homogeneous and inhomogeneous contributions, and MD simulations can be used to understand the molecular origins of the experimental data.[32,36,75] The full widths at half maximum (FWHMs) determined from molecular dynamics simulations show similar trends both for the two solutes and in different solvents although the line widths are somewhat smaller than those from experiments (Table SIII). Thus, the present QM/MM simulations can provide useful insights on properties of solvent dynamics.

Figure 2 shows the 2D-IR spectra at T_w = 0.3 ps (left column) and 3 ps (right column) for TriMOS in isopropanol (top row) and pentane (bottom row). All 2D-IR spectra acquired for both molecules in all solvents are provided in the supplementary material. An intuitive interpretation of these spectra is that the x-axis (ω_1) corresponds to the frequencies at which a subensemble of oscillators is excited by the first IR pulse and the y-axis (ω_3) is the range of frequencies that this subensemble exhibits after sampling its surroundings for a specific waiting time, T_w. Hence, the 2D-IR spectrum yields a frequency-frequency time correlation for the subensembles beneath the FTIR line shape.[31–34,36,76] Each spectrum has a positive-going (red) v = 0-1 peak that lies on or above the diagonal and a negative-going (blue) v = 1-2 peak that is shifted by the anharmonicity to lower frequencies along the ω_3 axis. A diagonal slice through the 0-1 peak reflects the range of frequencies captured by the linear FTIR line shape (assuming sufficient separation between the 0-1 and 1-2 peaks); the antidiagonal width represents the portion of the available frequencies that have been sampled during a given T_w period. This antidiagonal width contains contributions from very fast pure dephasing (T_2*) and relaxation (T_1), as well as spectral diffusion caused by the interconversion of molecular subensembles and driven by the reorganization of solvent molecules.[48,49,75]

For TriMOS, we observe in Figs. 2(a) and 2(b) that at short T_ws, the peak shape is diagonally elongated, indicating that the Si–H oscillators have not yet sampled the full

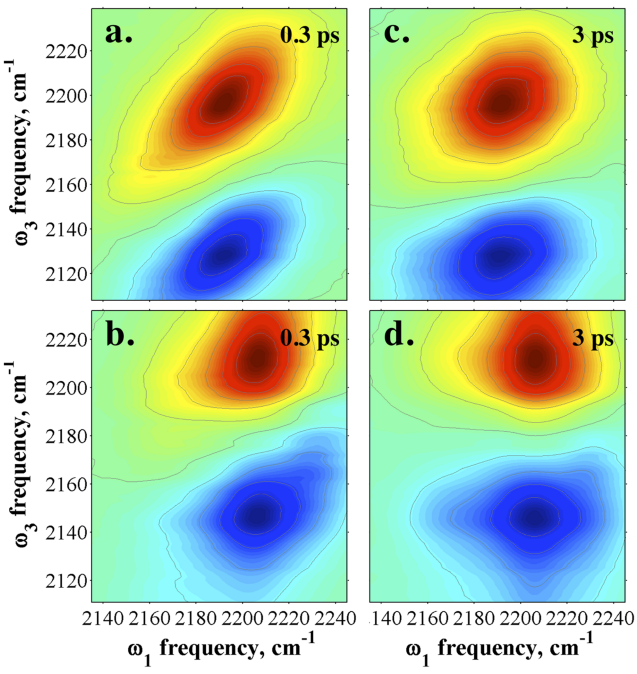

FIG. 2. 2D-IR spectra collected at T_w = 0.3 (left column) and 3 ps (right column) for the ν_{Si-H} mode on TriMOS in isopropanol [(a) and (c)] and pentane [(b) and (d)].

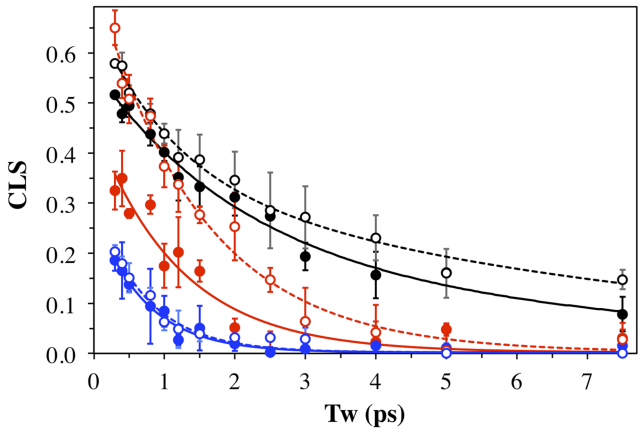

FIG. 3. CLS decays as a function of T_w for TriMOS (solid markers) and TriPS (open markers) in isopropanol (black), chloroform (red), and pentane (blue). Overlaid are solid curves (TriMOS) and dotted curves (TriPS) to show multiexponential fits to the data described in the text. The markers are the average CLS values, and the error bars are the standard deviations.

range of solvation environments. A comparison of these two contour plots reveals that the spectrum in isopropanol is more elongated along the diagonal direction than that in pentane; the Si–H mode of TriMOS has either sampled a greater range of the available solvent configurations in pentane than in isopropanol in the first 300 fs or there are less structural dynamics in the non-polar solvent. As the waiting time increases, the 2D-IR contour shapes become more circular, reflecting the loss of correlation due to spectral diffusion of the ν_{Si-H} oscillators [Figs. 2(c) and 2(d)]. By 3 ps, the 2D-IR spectral shape in pentane is nearly circular while some diagonal elongation persists in isopropanol at this T_w, revealing that the time scale of solvent shell rearrangements is slower in isopropanol.

To quantify these dynamic differences, we analyzed the centerline slope (CLS) for the v = 0-1 peaks at all T_ws for both molecules in all three solvents. Figure 3 shows the CLS values as a function of T_w along with multiexponential fits for TriMOS and TriPS in isopropanol, chloroform, and pentane. The CLS decays in isopropanol can be adequately represented by a double exponential fit for both TriMOS and TriPS, while a single exponential function is sufficient for the CLS decays in chloroform and pentane. This suggests that the solvent dynamics in chloroform and pentane enable all of the Si–H oscillators for both TriMOS and TriPS to experience all of the available frequencies under the linear line shape by about 5 ps. In contrast, some ν_{Si-H} oscillators remain partially correlated with their starting frequencies in isopropanol for both molecules since the CLS decays have not yet reached the baseline.

The CLS decays represent the normalized FFCFs, but they can be used to obtain the full FFCFs by iteratively fitting the CLS decays and the linear line shapes,[48,49] thereby separating the homogeneous and inhomogeneous contributions to the FTIR spectra. The resulting FFCF parameters are given in Table I and can be categorized as unresolvably fast spectral diffusion (Γ), fast spectral diffusion (~1 ps), and slow spectral diffusion (~10 ps). Vibrational dynamics are the fastest and the lowest amplitude in pentane, characteristic of a solvent that interacts very weakly with itself and couples very weakly to the ν_{Si-H} mode. Polar and strongly interacting solvents such as chloroform (weak H-bond donor) and isopropanol (strong H-bond donor and acceptor) exhibit slower, larger amplitude frequency fluctuations in the FFCF. The homogeneous line widths are similar for molecules in the same solvent and track inversely with the solvent polarity. Pentane exhibits the widest homogeneous line widths for both solute molecules, despite having the narrowest FTIR peak widths; the ν_{Si-H} mode in TriPS is more homogeneously broadened. The FTIR line shapes in chloroform and isopropanol are dominated by inhomogeneous broadening.

Interestingly, the amplitudes are statistically greater for TriMOS than TriPS in isopropanol and chloroform. The time scales of the dynamics sensed by these two species are the same, but they apparently have a larger influence on the Si–H mode for TriMOS. We have hypothesized previously that specific solvent-solute interactions with the oxygen atoms bound to a silicon site might be responsible for the enhanced solvatochromism in molecules such as TriMOS.[72,77] However, the FFCFs presented here for TriMOS, which has oxygen-bearing ligands, and TriPS, which lacks oxygen atoms, disprove this hypothesis since ν_{Si-H} on both molecules senses the same dynamics. Recall that DFT calculations above showed that enhanced solvatochromism arises from increased coupling of ν_{Si-H} to the reaction field due to mode polarization by the substituents. Here, we find that this polarization also enhances spectral diffusion.

The FFCFs for ν_{Si-H} on TriPS and TriMOS in isopropanol also exhibit a similar, slower dynamic contribution (Δ_2 and τ_2). Since the hydrogen atom of the Si–H group carries a negative partial charge (Table SII), it is not expected to donate a hydrogen bond to isopropanol, and such binding interactions have not been observed in silanes.[69] Similarly, hydrogen bonding interactions with the ligands are also ruled out by the lack of a

TABLE I. FFCF parameters for TriPS and TriMOS in isopropanol, chloroform, and pentane.

Solute	Solvent	Δ_1 (cm^{-1})[a]	τ_1 (ps)[b]	Δ_2 (cm^{-1})[a]	τ_2 (ps)[b]	Γ (cm^{-1})[a]
TriMOS	Isopropanol	16 (±4)	2.0 (±0.5)	12 (±4)	7 (±2)	6 (±2)
	Chloroform	23 (±5)	1.2 (±0.2)	...	...	7 (±3)
	Pentane	10 (±4)	0.7 (±0.1)	...	...	13 (±2)
TriPS	Isopropanol	8 (±3)	1.1 (±0.6)	8 (±2)	8 (±3)	5 (±1)
	Chloroform	15 (±2)	1.5 (±0.09)	...	...	6.1 (±0.7)
	Pentane	8 (±1)	0.72 (±0.07)	...	...	7.9 (±0.2)

[a]Errors show the range of which that parameter could be increased while the other parameters floated to fit the FTIR line shape 98% as well as the best value.
[b]Standard error of the exponential fit.

TABLE II. Computed FFCF parameters for TriPS and TriMOS in the three solvents.

Solute	Solvent	Δ_1 (cm^{-1})	τ_1 (ps)	Δ_2 (cm^{-1})	τ_2 (ps)	Δ_3 (cm^{-1})	τ_3 (ps)
TriMOS	Isopropanol	6.8	1.4	3.8	9.3	28.1	0.06
	Chloroform	6.6	1.7	...	...	25.1	0.07
	Pentane	3.3	1.9	...	...	27.1	0.06
TriPS	Isopropanol	9.3	0.90	5.0	6.3	30.4	0.06
	Chloroform	10.3	1.67	...	...	32.4	0.08
	Pentane	8.9	0.84	...	...	29.56	0.06

hydrogen-bond acceptor in TriPS. Consequently, we attribute the slower component to the hydrogen bonding dynamics of isopropanol with itself since the time scale is similar to what has been reported.[78–81] To confirm this hypothesis, we computed the FFCFs from QM/MM simulations, which were fitted to a combination of three exponentials plus a constant offset. Overall, the parameters obtained from the computed FFCFs (Table II) are in accord with those determined from experiment (Table I). Similar to experiment, both probes in isopropanol required two additional inhomogeneous exponential terms to describe the FFCF, while all of the other FFCFs only required one. Additionally, the time constants for the second exponential are in reasonable accord with the lifetime of hydrogen bonds.[78–81] The third exponential contains dynamics that are motionally narrowed and would contribute to the homogeneous line width (Γ).

The fast inhomogeneous spectral diffusion component (Δ_1 and τ_1) is ascribed to collective motions of bulk solvent molecules approximately resembling a dielectric continuum. Here, solvent molecules are indistinguishable, and coherent movement of the collection together leads to a variance in the electric field that is higher than the noise of the individual molecules. Spectral diffusion can be modeled here as a time-dependent Stark effect: the motions that lead to the largest variance in the electric field on the mode are those that contribute most strongly to the FFCF and are the basis for attribution of the signal lifetimes.

The FFCFs for the simulated solutes in isopropanol require a component (Δ_2 and τ_2) with a correlation time that is longer than the continuum motions. This is attributed to the reorganization of the isopropanol hydrogen bond network. It cannot be due to hydrogen bonding with the solute since it is present in the TriPS/isopropanol system as well. The hydrogen bond lifetime (τ_{HB}) of isopropanol was calculated as described in Sec. II. Table III presents the τ_{HB} values for the first solvation shell molecules (defined as having a distance less than 6.0 Å to the solute) around TriMOS and TriPS, as well as for the bulk solvent. Hydrogen bonds exchange faster in the bulk solvent, but τ_{HB} of the first solvation shell species are more relevant to the FFCF of ν_{Si-H} on the solutes. τ_{HB} in the solvation shell are in excellent agreement with τ_2 in the FFCFs obtained by MD simulations, strongly supporting the assignment that τ_2 dynamics in the experimental FFCFs originate from solvent shell hydrogen bond dynamics.

TABLE III. Hydrogen bond lifetimes (τ_{HB}) in isopropanol simulations.

Solvent environment	$\tau_{HB/bulk}$ (ps)	$\tau_{HB/first\ shell}$ (ps)
Trimos/isopropanol	4.15	9.3
TriPS/isopropanol	4.18	8.3
Bulk isopropanol	4.88	...

The autocorrelation functions of solvent dipole moments [dipole autocorrelation functions (DAFs)] were calculated for individual solvent molecules in the solvation shell around TriMOS and TriPS (Fig. 4). Because the bond lengths of the solvent molecules are constrained using SHAKE,[82] the DAFs only contain angle bending, torsional modes, and rotational motions of each solvent molecule. Isopropanol and chloroform both display exponential decay behavior, characteristic of rotational motions. Pentane shows damped oscillatory behavior, suggesting that the DAF is dominated by torsional and bending modes rather than rotation. The DAFs of chloroform and isopropanol were fitted to a sum of three and four exponentials, respectively, to adequately quantify the dipole dynamics (Table IV).

The DAF parameters for chloroform and isopropanol show the largest contribution to decorrelation from the slowest process (Table IV), which we attribute to the rotation of the whole molecule. Of the two solvents, molecular rotation in chloroform is significantly faster than that in isopropanol since chloroform is smaller, more spherical, and lacks restriction by hydrogen bonding interactions. Previous deuteron scattering studies reported that the rotational correlation times for deuterated isopropanol and $CDCl_3$ differed by a factor of 6,[83] which is relatively consistent with the slowest time coefficients obtained from the DAFs. Isopropanol displays two longer lifetimes of ~32 ps and ~92 ps that we tentatively attribute to

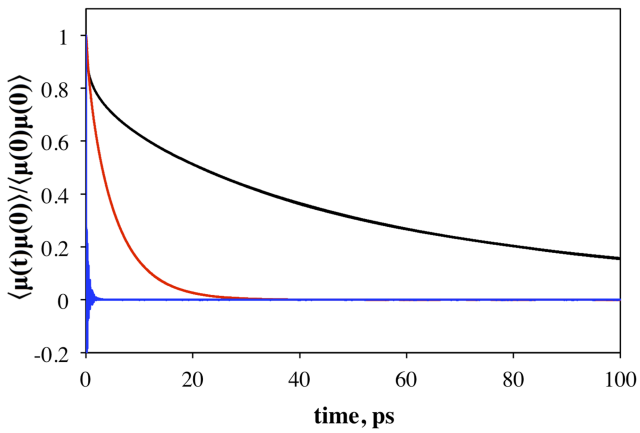

FIG. 4. Normalized dipole autocorrelation function (DAF) for individual solvent molecules in isopropanol (black), chloroform (red), and pentane (blue).

TABLE IV. Fitted parameters to the computed molecular dipole autocorrelation functions for TriMOS and TriPS in chloroform and isopropanol solutions.

Chloroform				Isopropanol			
TriMOS		TriPS		TriMOS		TriPS	
A	τ (ps)	A	τ (ps)	A	τ (ps)	A	τ (ps)
0.80	5.85	0.78	5.89	0.36	99.41	0.48	86.26
0.12	1.76	0.13	2.18	0.38	35.70	0.28	27.42
0.09	0.46	0.24	0.51	0.11	4.09	0.11	3.04
...	...	...	...	0.12	0.34	0.12	0.27

rotational motions within a hydrogen bonded network. These assignments are consistent with experimental rotational correlation times of 22 ps and 91 ps that were measured by NMR[83,84] and dielectric spectroscopies,[84,85] respectively. Meanwhile, we conjecture that the shortest lifetime (~0.4 ps) is dominantly due to fast intramolecular motions such as angle bending or dihedral rotations.

Isopropanol also contains a time coefficient that is comparable to the hydrogen bond lifetime. A similar value has been reported in the rotational correlation times measured by dielectric spectroscopy.[86] The largest DAF lifetime in isopropanol is on the order of 100 ps, indicating that there is no significant rotation of the dipole when isopropanol exchanges hydrogen bonds. This is most likely due to the size of isopropanol. The lifetime that is on the same order as the hydrogen bond lifetime only accounts for about 10% of the change in dipole. Furthermore, the large amount of time it takes for isopropanol to rotate suggests that it is hindered by hydrogen bonding interactions. Isopropanol maintains its orientation for a long time by exchanging hydrogen bonds with a close neighbor.

IV. CONCLUSIONS

Proper interpretation of static and time-resolved vibrational spectroscopic data requires understanding of the ways in which homogeneous and inhomogeneous effects are manifested in spectral change. In this study, TriMOS and TriPS provided an opportunity to monitor the same probe, the Si–H vibrational mode, with two different ligand sets and three solvent systems by steady-state FTIR and time-resolved 2D-IR spectroscopies. DFT calculations provided insight into the differences in silicon hydride sensitivity to the solvent through increased mode polarization with more electron withdrawing ligands. Calculations and simulations revealed that the solvatochromic trends of the hydride mode arise from specific hydrogen and halogen bonding interactions with the solute. Spectral diffusion experienced by ν_{Si-H} was found to be characteristic of the solvent type rather than the solute structure, yet it showed the same sensitivity observed in the FTIR solvatochromic shifts. Therefore, the solvent motions are dominated by their interactions with neighboring solvent molecules rather than with the solute. MD simulations confirmed that the dynamics experienced in isopropanol were due to hydrogen bonding fluctuations in the surrounding solvation shell. This was further corroborated by the calculation of the dipole autocorrelation function of individual solvent molecules throughout the bulk. These results showed the principle motions experienced by isopropanol molecules, which included a lifetime of similar magnitude to the hydrogen bonding lifetime. The remaining motions include rotational diffusion and low frequency intramolecular motions.

SUPPLEMENTARY MATERIAL

See supplementary material for details of 2D-IR and IR pump-probe measurements and FFCF determination, molecular dynamics (MD) simulations details and quantum vibrational perturbation (QVP) analysis, additional discussion about M06 calculations and solvatochromism, tabulated normal mode analysis results and CHELP charges, tabulated experimental and calculated FTIR peak parameters, computed linear absorption spectra from simulations, dihedral angle analysis of Si–H vibrational frequency, computed FFCFs from AM1/CHARMM simulations, DFT efforts to test specific interactions with TriMOS, tabulated normal mode analysis of TriMOS with explicit hydrogen bond donors, optimized configurations with H-bond donors, radial distribution function between H-bond donor and TriMOS, instantaneous frequencies versus VDW force on normal mode, and all experimental 2D-IR spectra in all solvents studied.

ACKNOWLEDGMENTS

The authors gratefully acknowledge partial support from the National Science Foundation under Grant Nos. CHE-0847356 and CHE-1464416 (to A.M.M.), the National Natural Science Foundation of China under Grant No. 21533003, and the National Institutes of Health under Grant No. GM46376 (to J.G.). C.M.O. and I.C.S. were supported by a National Science Foundation Graduate Student Research Fellowship Grant No. 00039202. Any opinions, findings, and conclusions or recommendations expressed in this material are those of the author(s) and do not necessarily reflect the views of the National Science Foundation.

[1] E. W. Castner and M. Maroncelli, J. Mol. Liq. **77**, 1 (1998).
[2] T. H. Joo, Y. W. Jia, J. Y. Yu, M. J. Lang, and G. R. Fleming, J. Chem. Phys. **104**, 6089 (1996).
[3] O. H. Kwon, T. H. Yoo, C. M. Othona, J. A. Van Deventer, D. A. Tirrell, and A. H. Zewail, Proc. Natl. Acad. Sci. U. S. A. **107**, 17101 (2010).
[4] R. M. Stratt and M. Maroncelli, J. Phys. Chem. **100**, 12981 (1996).
[5] R. A. Marcus, Rev. Mod. Phys. **65**, 599 (1993).
[6] P. F. Barbara, T. J. Meyer, and M. A. Ratner, J. Phys. Chem. **100**, 13148 (1996).
[7] C. P. Casey, S. E. Beetner, and J. B. Johnson, J. Am. Chem. Soc. **130**, 2285 (2008).
[8] P. B. Chock and J. Halpern, J. Am. Chem. Soc. **88**, 3511 (1966).
[9] R. Ugo, A. Pasini, A. Fusi, and S. Cenini, J. Am. Chem. Soc. **94**, 7364 (1972).
[10] G. Cainelli, P. Galletti, and D. Giacomini, Chem. Soc. Rev. **38**, 990 (2009).
[11] J. L. Gao, Acc. Chem. Res. **29**, 298 (1996).
[12] M. Brunori, F. Cutruzzola, C. Savino, C. Travaglini-Allocatelli, B. Vallone, and Q. H. Gibson, Trends Biochem. Sci. **24**, 253 (1999).
[13] T. A. Jackson, M. Lim, and P. A. Anfinrud, Chem. Phys. **180**, 131 (1994).
[14] K. A. Merchant, W. G. Noid, R. Akiyama, I. J. Finkelstein, A. Goun, B. L. McClain, R. F. Loring, and M. D. Fayer, J. Am. Chem. Soc. **125**, 13804 (2003).
[15] A. Ostermann, R. Waschipky, F. G. Parak, and G. U. Nienhaus, Nature **404**, 205 (2000).
[16] J. Z. Pu, J. L. Gao, and D. G. Truhlar, Chem. Rev. **106**, 3140 (2006).
[17] M. Karplus, J. Phys. Chem. B **104**, 11 (2000).

[18]V. Farina, B. Krishnan, D. R. Marshall, and G. P. Roth, J. Org. Chem. **58**, 5434 (1993).
[19]P. A. Fitzpatrick and A. M. Klibanov, J. Am. Chem. Soc. **113**, 3166 (1991).
[20]R. Riva, S. Schmeits, C. Jerome, R. Jerome, and P. Lecomte, Macromolecules **40**, 796 (2007).
[21]T. C. Schutt, V. S. Bharadwaj, G. A. Hegde, A. J. Johns, and C. M. Maupin, Phys. Chem. Chem. Phys. **18**, 23715 (2016).
[22]B. H. Jones, C. J. Huber, I. C. Spector, A. M. Tabet, R. L. Butler, Y. Hang, and A. M. Massari, J. Chem. Phys. **142**, 212441 (2015).
[23]L. M. Kiefer and K. J. Kubarych, J. Phys. Chem. A **119**, 959 (2015).
[24]R. A. Farrer and J. T. Fourkas, Acc. Chem. Res. **36**, 605 (2003).
[25]A. A. Jaye, N. T. Hunt, and S. R. Meech, J. Chem. Phys. **124**, 024506 (2006).
[26]H. Shirota, T. Fujisawa, H. Fukazawa, and K. Nishikawa, Bull. Chem. Soc. Jpn. **82**, 1347 (2009).
[27]M. H. Cho, S. J. Rosenthal, N. F. Scherer, L. D. Ziegler, and G. R. Fleming, J. Chem. Phys. **96**, 5033 (1992).
[28]F. Cichos, A. Willert, U. Rempel, and C. Von Borczyskowski, J. Phys. Chem. A **101**, 8179 (1997).
[29]B. Luther, J. Kimmel, and N. Levinger, J. Chem. Phys. **116**, 3370 (2002).
[30]M. Maroncelli, J. Mol. Liq. **57**, 1 (1993).
[31]C. R. Baiz, P. L. McRobbie, J. M. Anna, E. Geva, and K. J. Kubarych, Acc. Chem. Res. **42**, 1395 (2009).
[32]M. D. Fayer, Annu. Rev. Phys. Chem. **60**, 21 (2009).
[33]B. H. Jones and A. M. Massari, J. Phys. Chem. B **117**, 15741 (2013).
[34]M. Khalil, N. Demirdoven, and A. Tokmakoff, J. Phys. Chem. A **107**, 5258 (2003).
[35]D. F. Underwood and D. A. Blank, J. Phys. Chem. A **107**, 956 (2003).
[36]P. Hamm, M. H. Lim, and R. M. Hochstrasser, J. Phys. Chem. B **102**, 6123 (1998).
[37]I. J. Finkelstein, A. Goj, B. L. McClain, A. M. Massari, K. A. Merchant, R. F. Loring, and M. D. Fayer, J. Phys. Chem. B **109**, 16959 (2005).
[38]G. R. Medders and F. Paesani, J. Phys. Chem. Lett. **5**, 2897 (2014).
[39]P. A. Pieniazek, Y. S. Lin, J. Chowdhary, B. M. Ladanyi, and J. L. Skinner, J. Phys. Chem. B **113**, 15017 (2009).
[40]W. G. Rothschild, Mol. Phys. **105**, 1003 (2007).
[41]J. B. Asbury, T. Steinel, C. Stromberg, S. A. Corcelli, C. P. Lawrence, J. L. Skinner, and M. D. Fayer, J. Phys. Chem. A **108**, 1107 (2004).
[42]A. A. Bakulin, C. Liang, T. L. Jansen, D. A. Wiersma, H. J. Bakker, and M. S. Pshenichnikov, Acc. Chem. Res. **42**, 1229 (2009).
[43]J. D. Eaves, J. J. Loparo, C. J. Fecko, S. T. Roberts, A. Tokmakoff, and P. L. Geissler, Proc. Natl. Acad. Sci. U. S. A. **102**, 13019 (2005).
[44]Z. Ganim, H. S. Chung, A. W. Smith, L. P. Deflores, K. C. Jones, and A. Tokmakoff, Acc. Chem. Res. **41**, 432 (2008).
[45]M. B. Ji, M. Odelius, and K. J. Gaffney, Science **328**, 1003 (2010).
[46]S. Woutersen, Y. Mu, G. Stock, and P. Hamm, Chem. Phys. **266**, 137 (2001).
[47]B. H. Jones, C. J. Huber, and A. M. Massari, J. Phys. Chem. C **115**, 24813 (2011).
[48]K. Kwak, S. Park, I. J. Finkelstein, and M. D. Fayer, J. Chem. Phys. **127**, 124503 (2007).
[49]K. Kwak, D. E. Rosenfeld, and M. D. Fayer, J. Chem. Phys. **128**, 204505 (2008).
[50]H. S. Tan, I. R. Piletic, and M. D. Fayer, J. Opt. Soc. Am. B **22**, 2009 (2005).
[51]B. H. Jones, C. J. Huber, and A. M. Massari, J. Phys. Chem. A **117**, 6150 (2013).
[52]M. J. Frisch, G. W. Trucks, H. B. Schlegel, G. E. Scuseria, M. A. Robb, J. R. Cheeseman, G. Scalmani, V. Barone, B. Mennucci, G. A. Petersson, H. Nakatsuji, M. Caricato, X. Li, H. P. Hratchian, A. F. Izmaylov, J. Bloino, G. Zheng, J. L. Sonnenberg, M. Hada, M. Ehara, K. Toyota, R. Fukuda, J. Hasegawa, M. Ishida, T. Nakajima, Y. Honda, O. Kitao, H. Nakai, T. Vreven, J. A. Montgomery, Jr., J. E. Peralta, F. Ogliaro, M. J. Bearpark, J. Heyd, E. N. Brothers, K. N. Kudin, V. N. Staroverov, R. Kobayashi, J. Normand, K. Raghavachari, A. P. Rendell, J. C. Burant, S. S. Iyengar, J. Tomasi, M. Cossi, N. Rega, N. J. Millam, M. Klene, J. E. Knox, J. B. Cross, V. Bakken, C. Adamo, J. Jaramillo, R. Gomperts, R. E. Stratmann, O. Yazyev, A. J. Austin, R. Cammi, C. Pomelli, J. W. Ochterski, R. L. Martin, K. Morokuma, V. G. Zakrzewski, G. A. Voth, P. Salvador, J. J. Dannenberg, S. Dapprich, A. D. Daniels, Ö. Farkas, J. B. Foresman, J. V. Ortiz, J. Cioslowski, and D. J. Fox, GAUSSIAN 09, Revision E.01, Gaussian, Inc., Wallingford, CT, USA, 2009.
[53]B. R. Brooks, C. L. Brooks, A. D. Mackerell, L. Nilsson, R. J. Petrella, B. Roux, Y. Won, G. Archontis, C. Bartels, S. Boresch, A. Caflisch, L. Caves, Q. Cui, A. R. Dinner, M. Feig, S. Fischer, J. Gao, M. Hodoscek, W. Im, K. Kuczera, T. Lazaridis, J. Ma, V. Ovchinnikov, E. Paci, R. W. Pastor, C. B. Post, J. Z. Pu, M. Schaefer, B. Tidor, R. M. Venable, H. L. Woodcock, X. Wu, W. Yang, D. M. York, and M. Karplus, J. Comput. Chem. **30**, 1545 (2009).
[54]B. R. Brooks, R. E. Bruccoleri, B. D. Olafson, D. J. States, S. Swaminathan, and M. Karplus, J. Comput. Chem. **4**, 187 (1983).
[55]R. J. Xue, A. Grofe, H. Yin, Z. X. Qu, J. L. Gao, and H. Li, J. Chem. Theory Comput. **13**, 191 (2017).
[56]D. T. Colbert and W. H. Miller, J. Chem. Phys. **96**, 1982 (1992).
[57]J. Echave and D. C. Clary, Chem. Phys. Lett. **190**, 225 (1992).
[58]J. C. Light, I. P. Hamilton, and J. V. Lill, J. Chem. Phys. **82**, 1400 (1985).
[59]K. Kwac, H. Lee, and M. H. Cho, J. Chem. Phys. **120**, 1477 (2004).
[60]R. J. Gowers and P. Carbone, J. Chem. Phys. **142**, 224907 (2015).
[61]D. C. Rapaport, Mol. Phys. **50**, 1151 (1983).
[62]N. Michaud-Agrawal, E. J. Denning, T. B. Woolf, and O. Beckstein, J. Comput. Chem. **32**, 2319 (2011).
[63]A. V. Marenich, C. J. Cramer, and D. G. Truhlar, J. Phys. Chem. B **113**, 6378 (2009).
[64]B. Mennucci, Wiley Interdiscip. Rev.: Comput. Mol. Sci. **2**, 386 (2012).
[65]S. D. Fried and S. G. Boxer, Acc. Chem. Res. **48**, 998 (2015).
[66]M. I. Batuev, A. D. Petrov, V. A. Ponomarenko, and A. D. Matveeva, Bull. Acad. Sci. USSR **5**, 1269 (1956).
[67]G. Lucovsky, Solid State Commun. **29**, 571 (1979).
[68]G. Lucovsky, R. J. Nemanich, and J. C. Knights, Phys. Rev. B **19**, 2064 (1979).
[69]A. L. Smith and N. C. Angelotti, Spectrochim. Acta **15**, 412 (1959).
[70]H. W. Thompson, Spectrochim. Acta **16**, 238 (1960).
[71]C. J. Huber and A. M. Massari, J. Phys. Chem. C **118**, 25567 (2014).
[72]C. J. Huber, T. C. Anglin, B. H. Jones, N. Muthu, C. J. Cramer, and A. M. Massari, J. Phys. Chem. A **116**, 9279 (2012).
[73]T. M. Beale, M. G. Chudzinski, M. G. Sarwar, and M. S. Taylor, Chem. Soc. Rev. **42**, 1667 (2013).
[74]P. Politzer, J. S. Murray, and T. Clark, Phys. Chem. Chem. Phys. **15**, 11178 (2013).
[75]P. Hamm and M. T. Zanni, *Concepts and Methods of 2D Infrared Spectroscopy* (Cambridge University Press, Cambridge, 2011).
[76]C. Kolano, J. Helbing, M. Kozinski, W. Sander, and P. Hamm, Nature **444**, 469 (2006).
[77]C. J. Huber, S. M. Egger, I. C. Spector, A. R. Juelfs, C. L. Haynes, and A. M. Massari, J. Phys. Chem. C **119**, 25135 (2015).
[78]L. Chuntonov, I. M. Pazos, J. Q. Ma, and F. Gai, J. Phys. Chem. B **119**, 4512 (2015).
[79]R. Laenen, G. M. Gale, and N. Lascoux, J. Phys. Chem. A **103**, 10708 (1999).
[80]D. E. Moilanen, D. Wong, D. E. Rosenfeld, E. E. Fenn, and M. D. Fayer, Proc. Natl. Acad. Sci. U. S. A. **106**, 375 (2009).
[81]S. Park, M. Odelius, and K. J. Gaffney, J. Phys. Chem. B **113**, 7825 (2009).
[82]J.-P. Ryckaert, G. Ciccotti, and H. J. C. Berendsen, J. Comput. Phys. **23**, 327 (1977).
[83]B. M. Fung and T. W. McGaughy, J. Chem. Phys. **65**, 2970 (1976).
[84]K. Lin, N. Y. Hu, X. G. Zhou, S. L. Liu, and Y. Luo, J. Raman Spectrosc. **43**, 82 (2012).
[85]S. Mashimo, S. Kuwabara, and K. Higasi, J. Chem. Phys. **90**, 3292 (1989).
[86]J. Barthel, K. Bachhuber, R. Buchner, and H. Hetzenauer, Chem. Phys. Lett. **165**, 369 (1990).